Research Article

A Novel Method to Broaden the Single-Mode Bandwidth of the Rectangular Waveguide

Tingting Xie [ID],[1] Xiaohe Cheng,[1] Yuan Yao [ID],[1] Yaohui Yang,[2] Ting Zhang,[2] Junsheng Yu,[1] and Xiaodong Chen[3]

[1]*Beijing Key Laboratory of Work Safety Intelligent Monitoring, School of Electronic Engineering, Beijing University of Posts and Telecommunications, Beijing 100876, China*
[2]*Science and Technology on Electronic Test & Measurement Laboratory, Qingdao 266555, China*
[3]*School of Electronic Engineering and Computer Science, Queen Mary University of London, London, UK*

Correspondence should be addressed to Yuan Yao; yaoy@bupt.edu.cn

In this paper, a new class of broadband and low-loss transmission line called slotted rectangular waveguide (SRW) is proposed and analyzed. The proposed SRW consists of the rectangular waveguide and the inverted low-loss slotline, which can selectively suppress the higher-order mode (TE20 mode) and broaden the single dominant mode (TE10 mode) bandwidth in a rectangular waveguide (RW). The design principle and transmission characteristics of the SRW are illustrated and analyzed in this work. The transmission dominant mode bandwidth of the proposed SRW is analyzed and compared with the classic rectangular waveguide (RW), in which the dominant mode bandwidth of 60–155 GHz (88.4% bandwidth) is broader than the RW bandwidth of 60–116 GHz (63%). Two feed structures that can excite the two operating bandwidths (W and D band) of them separately are also designed. The SRW and transition exhibit broadband and low-loss characteristics from 75 GHz to 155 GHz, in which the transmission loss is lower than 0.68 dB and the return loss is over 18 dB.

1. Introduction

With the ever-increasing development of microwave communication systems, the integration of broadband and multiband interconnections and components into the same device has widely been required [1]. The transmission line is essential for the practical use of systems and circuits operating over the megahertz-through-terahertz frequency range [2]. Transmission lines with broadband and low attenuation play a critical role in microwave and terahertz backhaul links, which inhabits a special status in wireless communication and test systems.

Rectangular waveguide (RW) has been the hot spot of intense research for over four decades. The rectangular waveguide generally has a higher Q factor, lower loss, and lower insertion against other transmission lines [3, 4]. The rectangular waveguide is applied to various microwave and terahertz backhaul links. Nevertheless, the rectangular waveguide is

limited in bandwidth: the low frequency is related to the cut-off frequency f_c and the higher frequency is limited to higher-order modes, e.g., TE20 mode, TE01 mode, and TE11 mode [3, 4]. According to the cut-off frequency formula in [4], the first higher-order mode is the TE20 mode. The transmission lines based on the dominant mode are inevitably affected by higher-order modes, limiting the development of wireless communication systems [4, 5]. Single-mode operation in a rectangular waveguide is very important since the existence of multi modes may arouse distortions of carried signals due to modal dispersion. A large number of higher-order modes causes different group velocities in the transmission line, leading to signal distortion, as shown in Figure 1. However, it can still be used as a transmission line when the higher-order mode power is low.

Single-mode operation is crucial to achieving high transmission efficiency and stable system performance, where tremendous efforts have been devoted to suppressing higher-
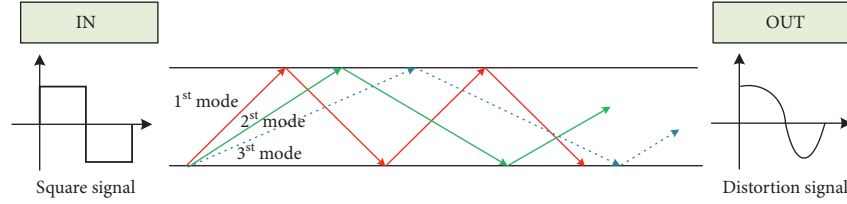
FIGURE 1: Signal distortion caused by the high-order mode of a transmission system.

order modes and improving single-mode bandwidth. Innovative waveguiding technology has been developed to fulfill all or part of these needs. A new version of the guide, called the ridge rectangular waveguide (Ridge RW), was proposed in [6, 7]. The role of the ridge is to increase the capacitance between the wide walls by reducing the size of the maximum E-field region parallel to the E-field. The advantages of ridge RWs compared to RWs are that these structures can maintain the characteristics of the waveguide, reduce the bandwidth of the cut-off frequency, and then broaden the single bandwidth of the dominant mode, which makes it have low loss and considerable bandwidth. However, the ridge waveguide suffers from the problem of process and integration. When working at high frequencies, the size of the ridge waveguide is relatively small, which makes it challenging to fabricate. In addition, the ridge waveguide is not easy to integrate with other planar transmission lines.

In this paper, we present a new method to broaden the single bandwidth of the dominant mode of RW. By cutting a long slot in the center of the longer side of the RW, called a slotted rectangular waveguide (SRW), with an inverted PCB substrate, the dominant mode bandwidth can be expanded from 60–116 GHz (63% bandwidth) to 60–155 GHz (88.4% bandwidth). This paper is organized as follows: the novel design of the SRW structure and the theoretical analysis are depicted in Section 2. Section 3 provides the results and discussions, and a brief conclusion is finally given in Section 4.

2. SRW Design and Theoretical Analysis

2.1. Structure of the Slotted Rectangular Waveguide (SRW). Figure 2 shows the schematic of the slotted rectangular waveguide, which consists of the rectangular waveguide and an inverted slotline. Furthermore, the two substrates are stacked to construct the transmission line. The inverted substrate is designed on a piece of Rogers 5880 substrate with $\varepsilon_r = 2.2$, $\tan \delta = 0.0009$, and $h_2 = 0.127$ mm. The slot on the embedded SRW is designed to disturb the current distribution of the RW, suppressing the higher-order mode (TE20 mode). We know that the width w2 of the waveguide slot causes radiation, affecting transmission loss and the single bandwidth of the dominant TE10 mode. Detailed values are listed in Table 1.

2.2. Operating Principle. According to the boundary conditions of the ideal conductor surface, the current density of the waveguide wall can be described as follows [3, 4]:

$$\vec{J}_s = \vec{e}_n \times \vec{H}, \tag{1}$$

where $\vec{e}_n$ is the unit vector of the normal direction outside the tube wall and $\vec{H}$ is magnetic field strength on the inner surface of the tube wall.

For the TEmn mode, the magnetic field component of the rectangular waveguide can be given by [3, 4, 8]

$$\begin{cases} H_z(x, y) & = H_m \cos\left(\dfrac{m\pi}{a}x\right)\cos\left(\dfrac{n\pi}{b}y\right)e^{-j\beta z}, \\[2mm] H_x(x, y, z) & = \dfrac{j\beta m\pi}{k_c^2 a}H_m \sin\left(\dfrac{m\pi}{a}x\right)\cos\left(\dfrac{n\pi}{b}y\right)e^{-j\beta z}, \\[2mm] H_y(x, y, z) & = \dfrac{j\beta n\pi}{k_c^2 b}H_m \cos\left(\dfrac{m\pi}{a}x\right)\sin\left(\dfrac{n\pi}{b}y\right)e^{-j\beta z}, \end{cases} \tag{2}$$

where H_m is the magnitude of the magnetic field, a and b are the width and height of the RW, $\beta = \sqrt{k^2 - k_c^2}$ is the propagation constant, and $k_c = \sqrt{(m\pi/a)^2 + (n\pi/b)^2}$ represents the cut-off wavenumber.

According to the method in [4, 8–10], the current of the waveguide wall can be solved by (1) and (2). The current distribution on the four sides of the waveguide can be divided into two cases, which are $x = 0$ and $y = 0$.

Case I: When $x = 0$, (2) results in

$$\begin{cases} H_z(0, y) = H_m \cos\left(\dfrac{n\pi}{b}y\right)e^{-j\beta z}, \\[2mm] H_x(0, y, z) = 0, \\[2mm] H_y(0, y, z) = \dfrac{j\beta n\pi}{k_c^2 b}H_m \sin\left(\dfrac{n\pi}{b}y\right)e^{-j\beta z}. \end{cases} \tag{3}$$

Also, by substituting (3) into (1), the current density of the waveguide wall can also be derived as

$$\begin{aligned} \vec{J}_s|_{x=0} &= \vec{e}_x \times \vec{H} \\[1mm] &= \vec{e}_x \times \left(\vec{H}_z + \vec{H}_y\right) \\[1mm] &= -\vec{e}_y H_z + \vec{e}_z H_y \\[1mm] &= -H_m \cos\left(\dfrac{n\pi}{b}y\right)e^{-j\beta z}\vec{e}_y + \dfrac{j\beta n\pi}{k_c^2 b}H_m \sin\left(\dfrac{n\pi}{b}y\right)e^{-j\beta z}\vec{e}_z. \end{aligned} \tag{4}$$

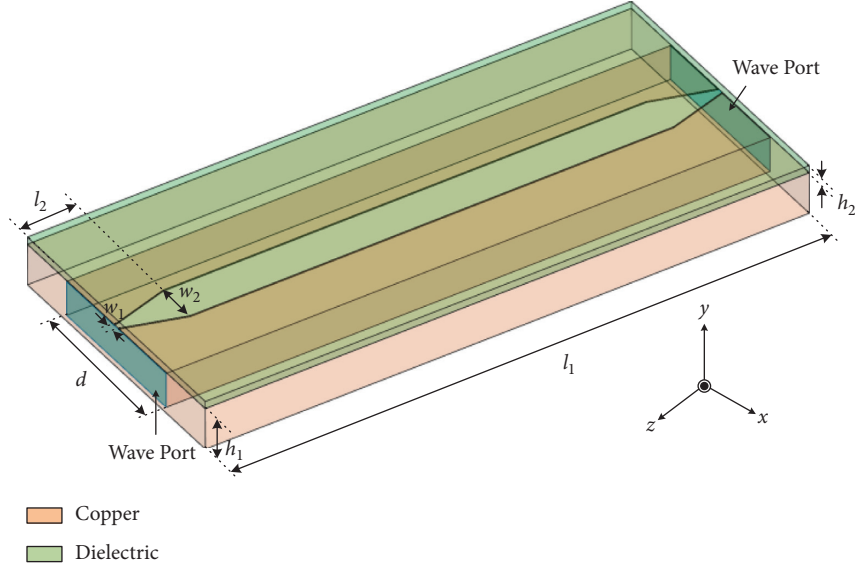Using the general root mean square average for the current, we obtain the following equation:

FIGURE 2: Schematics of the proposed SRW structure.

TABLE 1: Dimensions of the SRW and the feeding structure.

Parameter	d	w_1	w_2	h_1	h_2	l_1	l_2	l_3
Value (mm)	2.54	0.1	0.7	0.6	0.127	10	1	10
Parameter	l_4	x_1	x_2	x_3	y_1	y_2	y_3	l_5
Value (mm)	30	0.9	0.9	0.9	0.1	0.4	0.6	5
Parameter	l_6	l_7	x_4	x_5	x_6	y_4	y_5	y_6
Value (mm)	5	30	0.69	0.69	0.69	0.1	0.2	0.23

$$|\vec{J}|^2 = \frac{1}{2}H_m^2\cos^2\left(\frac{n\pi}{b}y\right) + \frac{1}{2}\left(\frac{\beta n\pi}{k_c^2 b}\right)^2 H_m^2 \sin^2\left(\frac{n\pi}{b}y\right)$$
$$= \frac{1}{2}H_m^2\left[\cos^2\left(\frac{n\pi}{b}y\right)\left(1 - \left(\frac{\beta n\pi}{k_c^2 b}\right)^2\right) + \left(\frac{\beta n\pi}{k_c^2 b}\right)^2\right]. \quad (5)$$

Therefore, when $\cos^2(n\pi/by) = 1$, $|\vec{J}|^2$ reach the max value

$$\begin{cases} n = 0, \\ y = 0, \\ y = b. \end{cases} \quad (6)$$

Note that $n = 0$ means TEm0 mode, e.g., TE10 and TE20 mode can reach maximum value. When $x = a$, we get the same results as above.

Case II: When $y = 0$, the (2) can be written by

$$\begin{cases} H_z(x,0) = H_m\cos\left(\frac{m\pi}{a}x\right)e^{-j\beta z}, \\ H_x(x,0,z) = \frac{j\beta m\pi}{k_c^2 a}H_m\sin\left(\frac{m\pi}{a}x\right)e^{-j\beta z}, \\ H_y(x,0,z) = 0. \end{cases} \quad (7)$$

By substituting (7) into (1), we have

$$\vec{J}_s|_{y=0} = \vec{e}_y \times \vec{H}$$
$$= \vec{e}_y \times \left(\vec{H}_z + \vec{H}_x\right)$$
$$= \vec{e}_x H_z - \vec{e}_z H_x$$
$$= H_m\cos\left(\frac{m\pi}{a}x\right)e^{-j\beta z}\vec{e}_x - \frac{j\beta m\pi}{k_c^2 a}H_m\sin\left(\frac{m\pi}{a}x\right)e^{-j\beta z}\vec{e}_z. \quad (8)$$

Similarly, these conditions can be expressed as

$$|\vec{J}|^2 = \frac{1}{2}H_m^2\cos^2\left(\frac{m\pi}{a}x\right) + \frac{1}{2}\left(\frac{\beta m\pi}{k_c^2 a}\right)^2 H_m^2\sin^2\left(\frac{m\pi}{a}x\right)$$
$$= \frac{1}{2}H_m^2\left[\cos^2\left(\frac{m\pi}{a}x\right)\left(1 - \left(\frac{\beta m\pi}{k_c^2 a}\right)^2\right) + \left(\frac{\beta m\pi}{k_c^2 a}\right)^2\right]. \quad (9)$$

When $\cos^2(m\pi/ax) = 1$, $|\vec{J}|^2$ reach the max value, we obtain the following result:

$$\begin{cases} m = 0, \\ m = 1 \text{ and } x = 0 \text{ or } a, \\ m = 2 \text{ and } x = \frac{a}{2} \text{ or } 0 \text{ or } a, \end{cases} \quad (10)$$

where $m = 0$ means the $|\vec{J}|^2$ of TE0n mode reaches a maximum value; $m = 1$ and $x = 0$ or a mean the $|\vec{J}|^2$ of TE10 mode can reach maximum when $x = 0$ or a; $m = 2$ and $x = a/2$ or 0. or a mean the $|\vec{J}|^2$ of TE20 mode can reach maximum when $x = a/2$ or 0 or a.

When $\cos^2(m\pi/ax) = 0$, $|\vec{J}|^2$ reach the min value.

$$\begin{cases} m = 1 \text{ and } x = \dfrac{a}{2}, \\[2mm] m = 2 \text{ and } x = \dfrac{a}{4} \text{ or } \dfrac{3a}{4}, \end{cases} \tag{11}$$

where $m = 1$ and $x = a/2$ means the $|\vec{J}|^2$ of TE10 mode can reach a minimum when $x = a/2$; $m = 2$ and $x = a/4$ or $3a/4$ mean the $|\vec{J}|^2$ of TE20 mode can reach a minimum when $x = a/4$ or $3a/4$. When $y = b$, we get the same result as above.

Above all, we can get the current amplitude of TE10 and TE20 modes [4, 8]. Based on the current distribution mechanism of the waveguide wall, the normalized current amplitude of TE10 and TE20 modes on all four sides of the waveguide are shown in Figure 3. It implies the shorter sides of RW reach their maximum, whether in TE10 mode or TE20 mode. It can be observed that when at $x = a/2$, the TE20 current amplitude reaches the maximum, whereas, the TE10 current amplitude reaches the minimum. Therefore, it is vital to suppress the current of TE20 mode at this position. Adding a slot to the longer waveguide $x = a/2$ can disturb the current distribution and affect the electromagnetic field. And, the field of TE20 mode can be suppressed or radiated in SRW, and then the single bandwidth of the dominant mode (quasi-TE10 mode) can be broadened.

3. Results and Discussion

The novel proposed broadband transmission line is simulated and optimized using a commercial full-wave electromagnetic solver Ansys HFSS [11].

3.1. Field Distribution. The yield field distribution of SRW and RW at different frequencies is presented, clearly distinguishing the dominant or higher-order modes [4, 12]. The phenomenon of broadening the single dominant mode bandwidth of RW with increasing frequency is observed, evidenced by the field distributions of various field components. The dimension of the RW is W-band size ($2.54\,\text{mm} \times 0.6\,\text{mm}$), and the single dominant band is 75–110 GHz. The field distribution curves depicted in Figures 4 and 5 are normalized maximum magnitudes of E field components and H field components, respectively, along the x-axis (0 mm to 2.54 mm) from 90 GHz to 150 GHz in increments of 20 GHz. The solid lines are the field distribution of SRW, and the dashed lines are the field distribution of RW. From Figure 4, the $|E_y|$ and $|H_x|$ curves of RW become approximately one half sinusoidal wave from 90 GHz to 110 GHz, and gradually appear one sinusoidal wave (TE20 mode) with increasing frequency whereas the $|E_y|$ and $|H_x|$ curves of SRW curves only have one half sinusoidal wave by increasing the frequency of operation, illustrating the higher-order mode (TE20 mode) is absent or rare in SRW. Furthermore, it is shown clearly that $|H_z|$ of RW has one half cosine wave at 75–110 GHz and increases one half cosine wave with increasing frequency. And the $|H_z|$ of SRW has one half cosine wave by increasing the frequency of operation, thereby making the whole curves approximately
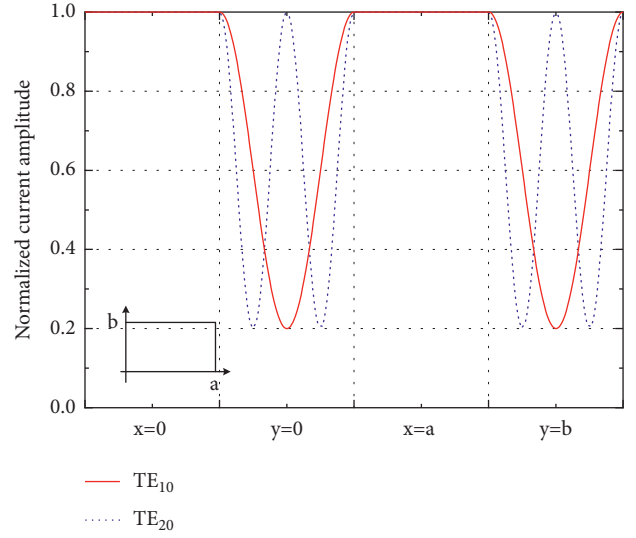

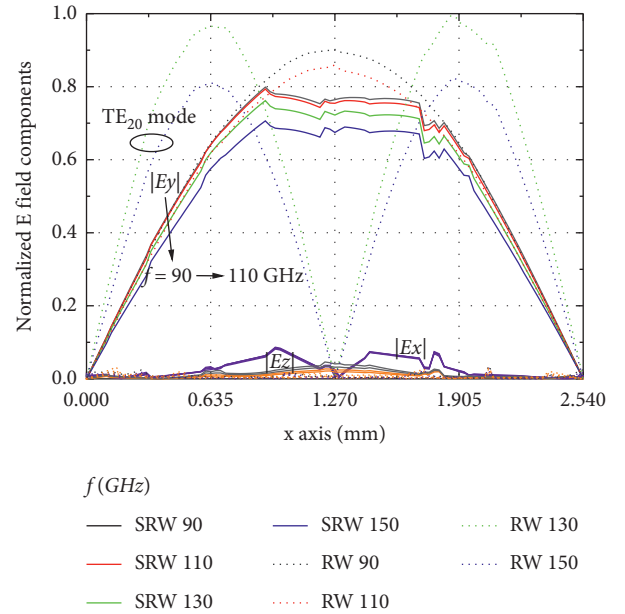FIGURE 3: Normalized current amplitude.

FIGURE 4: Normalized E field components distribution of SRW: (a) normalized $|H_x|$ and $|H_y|$ field components distribution and (b) normalized $|H_z|$ field component distribution.

suppress the higher-order mode (TE20 mode). Both $|E_x|$, $|E_z|$ and $|H_y|$ of SRW are as small as zero with increasing frequency, which agrees with the quasi-TE10 mode characteristics of RW. As the frequency continues to increase, these facts reveal that the field distributions of SRW resemble those of the fundamental mode TE10 from 75 GHz to 155 GHz.

To further explain this problem, Figure 6 is the sketched picture of the E-field distribution of RW and SRW at 150 GHz, in which the wave-ports of structures are only excited by the higher-order mode (TE20 mode) simultaneously. Figure 6 illustrates that the higher-order mode (TE20 mode) of SRW cannot be transmitted and excited
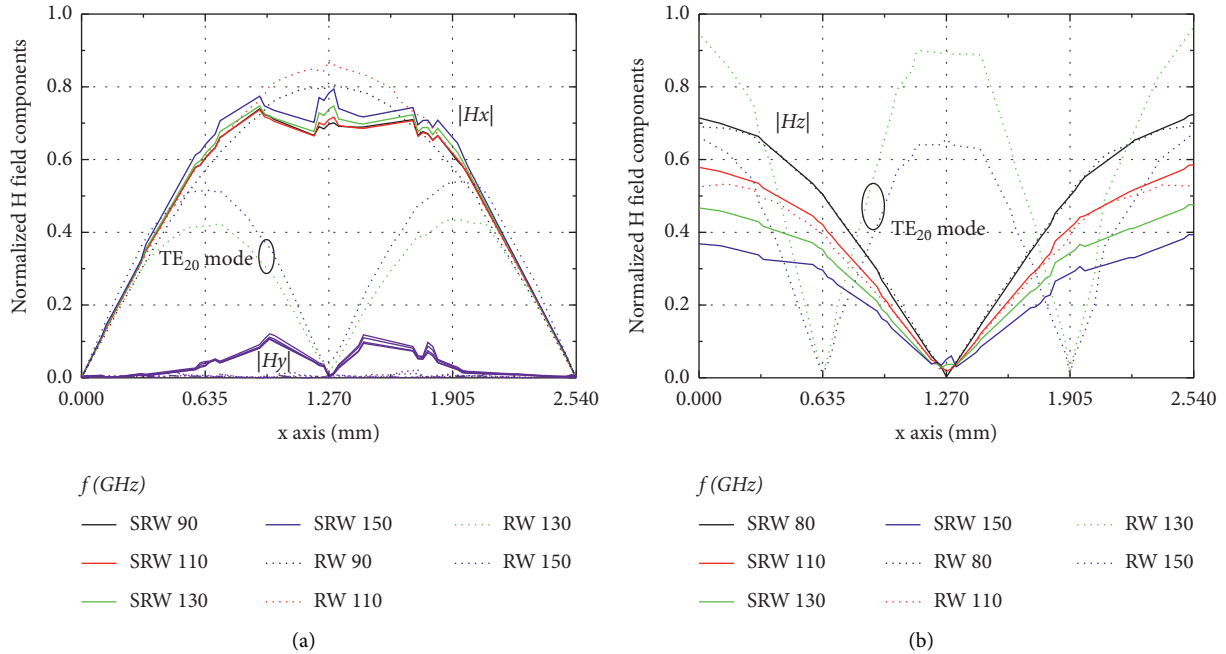
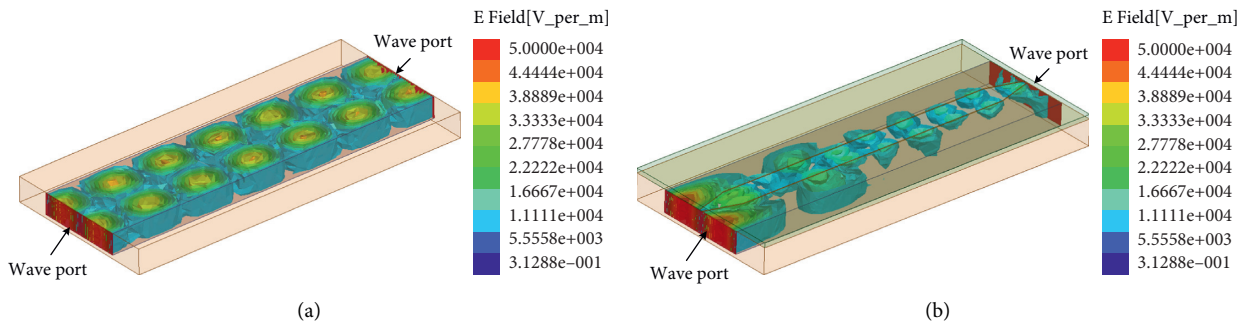FIGURE 5: Normalized H field components distributions of SRW: (a)$|H_x|$ and $|H_y|$ and (b)$|H_z|$.

FIGURE 6: RW and SRW are only excited by TE20 excitation: (a) the E field of RW at 150 GHz and (b) the E field of SRW at 150 GHz.

completely, whereas the TE20 mode of RW can be excited. These results reveal that SRW is difficult to excite by the higher-order mode (TE20 mode) due to the slot in SRW.

Above all, Figure 7 shows the dominant and higher-order mode transmission coefficient of the RW, SRW, and Ridge RW. The solid lines are the TE20 transmission, and the dashed lines are the TE10 transmission. The black line, red line, and blue line represent Ridge RW, RW, and SRW, respectively. The higher-order mode (TE20 mode) of the RW is excited at 116 GHz, and the higher-order mode of the SRW has a sudden downward trend at 116 GHz, where the higher-order mode (TE20 mode) is suppressed to −15 dB. The green dot-dashed line is the light line for the transmission coefficient of −15 dB. Deteriorating the transmission coefficient of the TE20 mode means that the higher-order mode (TE20 mode) is suppressed. Furthermore, the purple area is the dominant bandwidth of the RW (60–116 GHz), the green area is the dominant bandwidth of the Ridge RW (53–123 GHz), and the blue area is the dominant bandwidth of the SRW (60–155 GHz). The reason for the broadband of the ridge waveguide is that the cut-off frequency is lower than RW, and

the high-order mode is higher than RW. In summary, Table 2 compares the transmission characteristics of the various transmission lines. Compared with RW/Ridge RW, SRW has advantages in broadband. Due to the fact that RWs have a small size at high frequencies, the ridge waveguides are difficult to process at high frequencies. As mentioned above, the slot in SRW suppresses the higher-order mode (TE20 mode) and broadens the bandwidth of the dominant mode (TE10 mode).

3.2. Transmission Performances. Figure 8 shows the transmission coefficient of the TE10 mode and the TE20 mode for different dimensions of slot width w2. It can be observed that the width of slot w2 affects the transmission coefficient significantly, which results in deterioration insertion loss of TE10 mode and TE20 mode with slot w2 increasing. This means that the higher-order mode (TE20 mode) can be suppressed. However, the insertion loss of the dominant mode (TE10 mode) deteriorates with slot w2 increasing. To achieve low loss and broadband performance, we choose a
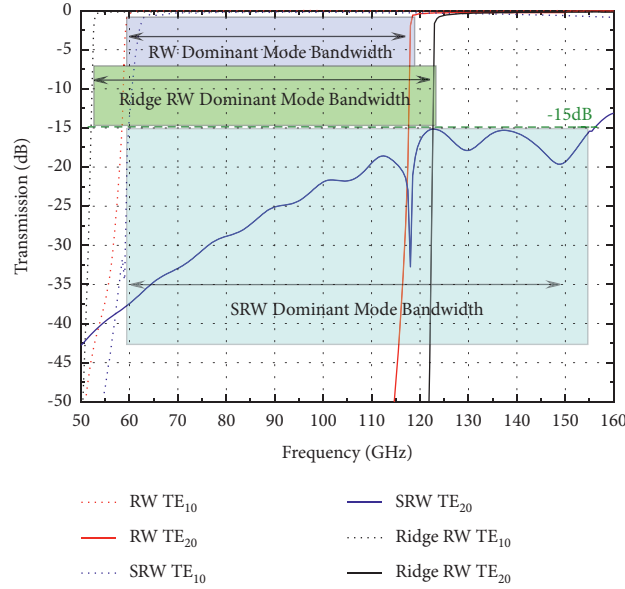
FIGURE 7: The dominant (TE10 mode) and high-order mode (TE20 mode) transmission coefficients of RW, SRW, and Ridge RW.

TABLE 2: Comparing the transmission characteristics of transmission lines.

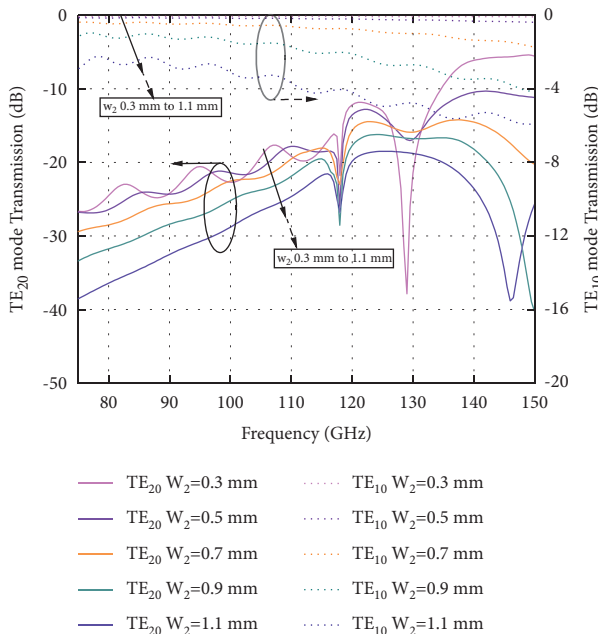| Type	Mode	Bandwidth (GHz)	Fabrication	Loss	Size
RW	TE_{10}	60–120 (66.7%)	Middle	Low	$0.847\ \lambda_0^* \times 0.2\ \lambda_0^*$
Ridge RW	TE_{10}	53–123 (79.35%)	Low freq: middle; high freq: hard	Low	$0.847\ \lambda_0^* \times 0.2\ \lambda_0^*$ (ridge height $0.07\ \lambda_0^*$)
SRW	TE_{10}	60–155 (88.4%)	Middle	Low	$0.847\ \lambda_0^* \times 0.2\ \lambda_0^*$

λ_0^* is the air wavelength at 100 GHz.

FIGURE 8: Simulated transmission coefficients of TE10 mode and TE20 mode for slot width w2 = 0.3, 0.5, 0.7, 0.9, and 1.1 mm.

suitable value of w2 to compromise between insertion loss and broadband. Finally, it is decided that w2 is 0.7 mm, which means the transmission of the high-order mode (TE20 mode) deteriorated by -15 dB, and it can be regarded

as the higher-order mode did not show up. In consideration of low loss, Figure 9 shows the |S|-parameters for the triangular and straight slots, respectively. Interestingly, good matching is achieved in the triangular slot for reflection coefficients below −20 dB and transmission coefficients are higher than −0.6 dB from 75 GHz to 155 GHz.

3.3. The Feeding Structure and Result. This section explains the impedance matching of the SRW. The transitions from standard waveguides to the SRW have been designed and optimized to verify the transmission characteristics. The transitions from standard waveguides to the SRW have been designed and optimized to verify the transmission characteristics. Since the operation bandwidth for the SRW is from 75–155 GHz, we need two transitions to different standard waveguides: one to the W band standard waveguide WR-10 and the other to the D band standard waveguide WR-7. Figure 10 is the geometry of the transmission line with Chebyshev impedance matching and feeding structure, which is a back-to-back structure. Here, the excited waveport used in HFSS is defined as the width and the height of standard RW, where the size is the same as WR-10 and WR-7. For the W&D band transition, the Chebyshev impedance matching structure with three stepped ridges is used, and then the height is changed to the standard waveguide by tapering, as shown in Figure 10. This gave a good match. The simulated results for this transition are shown in Figure 11, where the reflection coefficients are lower than −18 dB, and
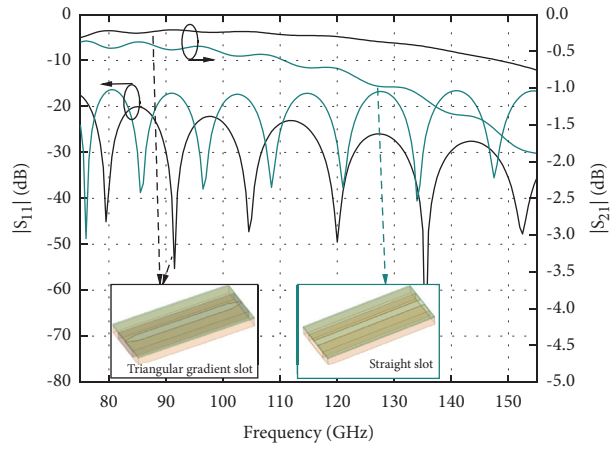
FIGURE 9: Simulated S-parameters of straight SRW and triangular gradient SRW.
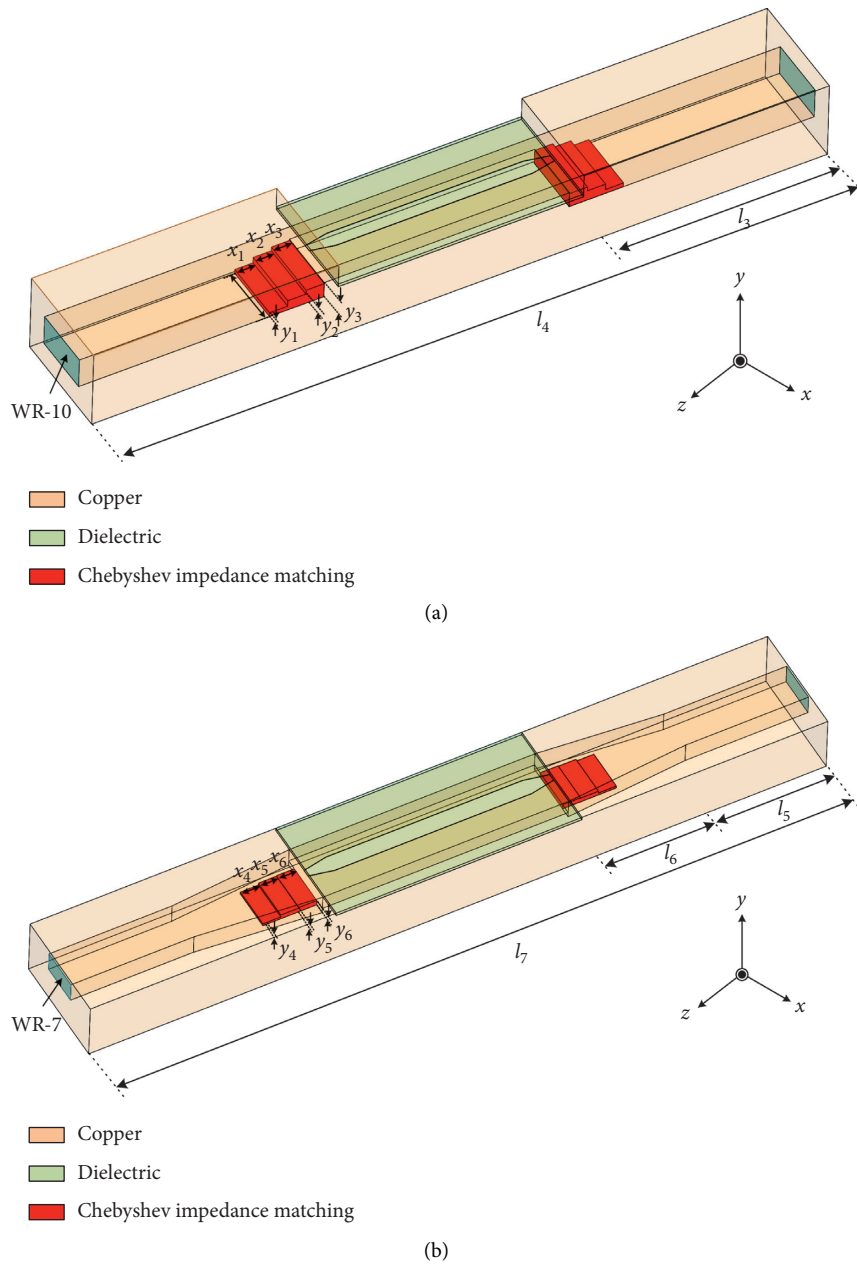

(a)

(b)

FIGURE 10: Two transitions from the SRW in Figure 2 to standard waveguides WR-10 and WR-7: (a) W band transition and (b) D band transition.
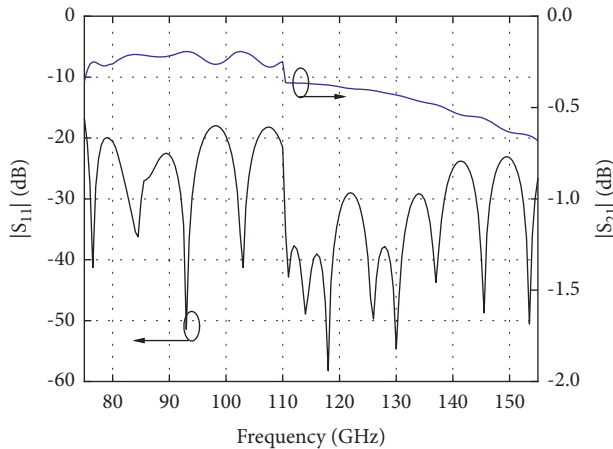
Figure 11: The simulated S parameters for the transitions between 75 and 155 GHz.

the transmission coefficients are higher than −0.68 dB over 75–155 GHz. All the values of the design parameters are given in Table 1, and excellent transmission can be obtained for these parameters.

4. Conclusions

We have presented a novel broadband transmission line for millimeter-wave applications. In the proposed concept, the slotted rectangular waveguide called SRW is constructed by an inverted slotline. The simulated performance and operating principles of the prototypes were presented to verify the performance of the proposed concept. Broadband and low-loss performance have been successfully achieved in a range from 60 GHz to 155 GHz (88.4% bandwidth) with the single dominant mode of TE10 transmission. Moreover, transitions of the SRW are also proposed with an insertion loss of 0.68 dB at 155 GHz. The higher-order mode of the RW shows critical bandwidth limitations that the slot of RW (SRW) suppresses the higher-order mode current and shows the potential to overcome. The proposed unique architecture opens up an opportunity to provide broadband and low-loss waveguide and devices. According to the transmission performance comparison of the classical RW, the proposed design is attractive in ultra-broadband wireless communications.

Data Availability

The data used to support the findings of this study are included in the article.

Conflicts of Interest

The authors declare that there are no conflicts of interest with this study.

Acknowledgments

References

[1] Z. Pi and F. Khan, "An introduction to millimeter-wave mobile broadband systems," *IEEE Communications Magazine*, vol. 49, no. 6, pp. 101–107, 2011.

[2] C. Caloz and T. Itoh, *Electromagnetic Metamaterials: Transmission Line Theory and Microwave Applications*, Wiley, New York, NY, USA, 2004.

[3] N. Marcuvitz, *Waveguide handbook*, pp. 399–402, McGraw-Hill, New York, NY, USA, 1951.

[4] D. M. Pozar, *Microwave Engineering*, Wiley, New York, NY, USA, 3rd edition, 2004.

[5] H. Soekmadji, S. Liao, and R. J. Vernon, "Experiment and simulation on TE10 cut-off reflection phase in gentle rectangular downtapers," *Progress In Electromagnetics Research Letters*, vol. 12, pp. 79–85, 2009.

[6] T.-S. Chen, "Calculation of the parameters of ridge waveguides," *IEEE Transactions on Microwave Theory and Techniques*, vol. 5, no. 1, pp. 12–17, 1957.

[7] S. B. Cohn, "Properties of ridge wave guide," *Proceedings of the IRE*, vol. 35, no. 8, pp. 783–788, 1947.

[8] C.-Q. Jiao, "Selective suppression of electromagnetic modes in a rectangular waveguide by using distributed wall losses," *Progress In Electromagnetics Research Letters*, vol. 22, pp. 119–128, 2011.

[9] B. Z. Katsenelenbaum, *High-Frequency Electrodynamics*, Wiley, Weinheim, Germany, 2006.

[10] C. Chongqing Jiao, "Shielding effectiveness improvement of metallic waveguide tube by using wall losses," *IEEE Transactions on Electromagnetic Compatibility*, vol. 54, no. 3, pp. 696–699, 2012.

[11] A. Corp and P. A. Canonsburg, "USA HFSS: High Frequency Structure Simulator Based on the Finite Element Method," 2021, http://www.ansoft.com.

[12] D. Wang, F. Fesharaki, and K. Wu, "Physical evidence of mode conversion along mode-selective transmission line," in *Proceedings of the 2017 IEEE MTT-S International Microwave Symposium (IMS)*, pp. 491–494, Honolulu, HI, USA, June. 2017.